

Characterization of Nitrogen-Boron doped 4H-SiC substrates

Rusheng Wei, Xiufang Chen, Lihuan Wang, Sheng Song, Kun Yang, Xiaobo Hu*, Yan Peng*,
Xiangang Xu

State Key Laboratory of Crystal Materials, Shandong University, Jinan, Shandong Province, 250100,
China

*E-mail: xbhu@sdu.edu.cn; penny4964@163.com

Received: 11 March 2013 / Accepted: 28 March 2013 / Published: 1 May 2013

Nitrogen-Boron doped 4H-SiC single crystal was prepared by physical vapor transport method and the doping concentration was determined by secondary ion mass spectroscopy. The resistivity of 4H-SiC substrate was measured by contactless method. It was found that the resistivity decreased from center to edge of the substrates. Carrier concentration distribution on 4H-SiC was simulated based on Raman spectra mapping. From center to edge, the carrier concentration decreased gradually. Photoluminescence spectra of 4H-SiC showed a peak wavelength of about 538 nm with full width at half maximum (FWHM) about 104 nm. The emission intensity is enhanced with the Nitrogen concentration increasing and then suppressed because of the free carrier absorption enhancement.

Keywords: silicon carbide, fluorescent, Raman spectra, photoluminescence

1. INTRODUCTION

White light-emitting diodes (LEDs) are very promising devices for illumination applications such as backlight source of liquid crystal flat display panels and the head lights of mobiles. One common method to get white LEDs is using a UV or blue LED over-coated with phosphor, such as yttrium aluminum garnet (Ce:YAG)[1]. These LEDs are already used as a light source in a variety of portable equipments. In principle, the white LED is a compact, robust and efficient light source. Therefore, it is believed that all conventional light sources can be replaced by white LEDs in the future. However, there are still some problems with the conventional white LEDs, such as low total flux and low color rendering index. These problems blocked the expansion of white LED applications [2].

For conventional white LED mentioned above, the color rendering index is very low due to lack of red phosphors. Three-color phosphors have also been developed to improve the color rendering property. However, this type of device has low emission efficiency due to the low efficiency of red phosphors. In addition, the combination of LED and phosphors has an intrinsic instability of color against temperature change. Moreover, complicated assembly processes are required to set the phosphors uniformly on the LED chip. Therefore, high-efficiency wavelength converters with high color rendering index (CRI) value and long lifetime are indispensable.

Silicon carbide (SiC) can emit light from near UV across the entire visible spectrum by introducing different dopants because of its wide band gap. Compared with the high-efficiency nitride-based visible and UV LEDs or emitters, [3-11] SiC based LED has relatively low light emission efficiency due to its indirect band gap. Recently, impurity-doped SiC materials have been applied in different fields [12-15]. For example, donor-and-acceptor (DA) doped SiC is a promising candidate phosphor for the fabrication of white LEDs since it can work as a high performance phosphor [16-18], i.e., a light-emission medium by optical pumping. As a phosphor, DA doped SiC has many advantages such as high thermal conductivity for high-power-operated LEDs and well-established substrate material for the epitaxial growth of nitride. Therefore, white LEDs with DA doped SiC are also expected to provide an excellent color rendering index.

In this paper, the Nitrogen (N) and Boron (B) doped 4H-SiC single crystal as DA doped fluorescent SiC substrates was prepared by physical vapor transport (PVT) method for the first time. Then the conductive and optical properties of the substrates were investigated. Raman spectroscopy and contactless resistivity measurement were used to determine the conductive properties of the substrates. Raman spectra mapping characterized the longitudinal optical phonon-plasmon coupled (LOPC) mode of the substrates, from which the carrier concentration distribution on the entire substrate could be simulated. Photoluminescence (PL) spectrum was investigated in order to explore the fluorescent properties of N-B doped 4H-SiC.

2. EXPERIMENTS

4H-SiC single crystal with the diameter of 2'' was grown by the modified Lely technique, i.e., by physical vapor transport (PVT) method in the temperature range of 2000-2200 °C. The growth was carried out on the C-face seed in a graphite crucible and the growth orientation was parallel to the c-axis. The crucible was heated by an inductive coil using a RF generator and SiC powder was put at the bottom of the crucible as the source. The growth pressure was 50 mbar and Argon was used as carrier gas. The temperature was measured on the top lid via a color pyrometer. B was introduced by mixing Boron Carbide (B_4C_3) in the SiC powder source and N was introduced by a N_2 gas flow during the growth. The single crystal ingots were then sliced parallel to the (0001) plane. After lapping and polishing, the 4H-SiC wafers were obtained.

3. RESULTS AND DISCUSSION

Secondary Ion Mass Spectroscopy (SIMS) was carried out to determine the N and B doping concentration. The testing points were positioned at the center of the wafer in our experiments. The results showed that the concentration of N and B was $1.1 \times 10^{19} \text{cm}^{-3}$ and $4.2 \times 10^{18} \text{cm}^{-3}$ at the center, respectively.

Contactless resistivity measurements were carried out with a Model EC-80P system as shown in Fig.1. We selected five testing points a, b, c, d and e from one radius. The distance of the points away from the center were 0 mm, 5 mm, 10 mm, 15 mm, 20 mm, respectively. We can see that the resistivity of N-B doped 4H-SiC increases monotonously from center to edge across the wafer.

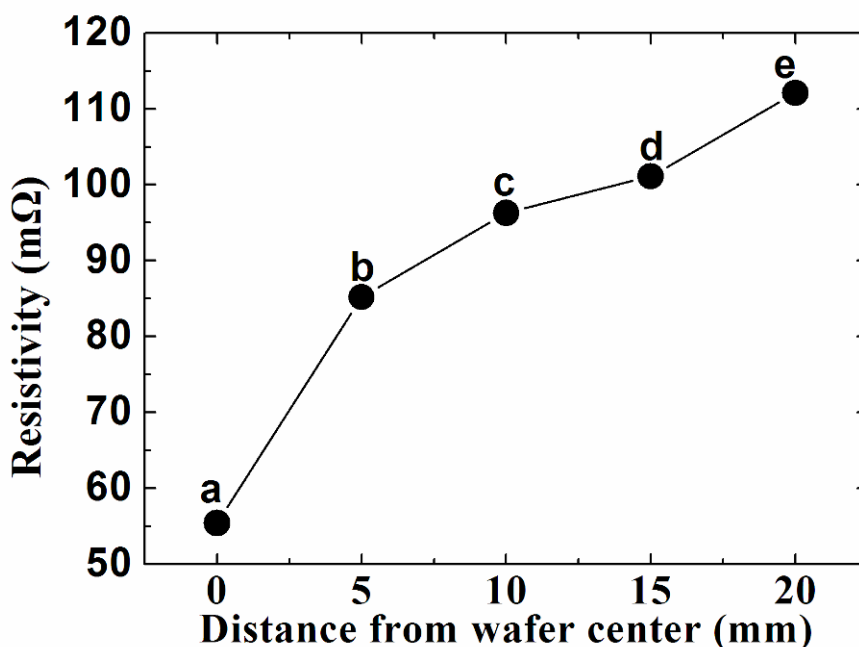


Figure 1. Resistivity measurement results of points a, b, c, d and e.

Raman scattering spectra of the N-B doped 4H-SiC wafers were collected in a back-scattering configuration by a HR 800 system from Horiba Jobin Yvon. A 532 nm laser (40 mW) was used as excitation source, the interval of mapping points was 2 mm. The grating we used was 600 g/mm and the expose time was 1 second.

In n-type DA doped 4H-SiC, the predominant mechanism for the Raman shift of LO mode is the coupling interaction between LO phonons and overdamped plasmons [19-25].

The Plasmon frequency ω_p is given by

$$\omega_p = \left(\frac{4\pi n e^2}{\epsilon_\infty m^*} \right)^{1/2} \tag{1}$$

where ϵ_∞ is the optical dielectric constant, n is the concentration of free electrons and m^* is the electron effective mass. The LO mode is then redefined as LOPC mode. The LOPC modes of a, b, c, d and e were shown in Fig. 2.

From Eq. (1), one can see that ω_p is proportional to \sqrt{n} , so the plasmon frequency increases with the increase of the free electron concentration, and the peak position of LOPC mode shifts toward higher wavenumbers, which are caused by an enhancement of coupling interaction between phonons and plasmons, as shown in Fig. 3a. In the meanwhile, the intensity of LOPC mode decreases as shown in Fig. 3b. And the full width at half maximum (FWHM) of LOPC mode is broaden, as shown in Fig. 3c.

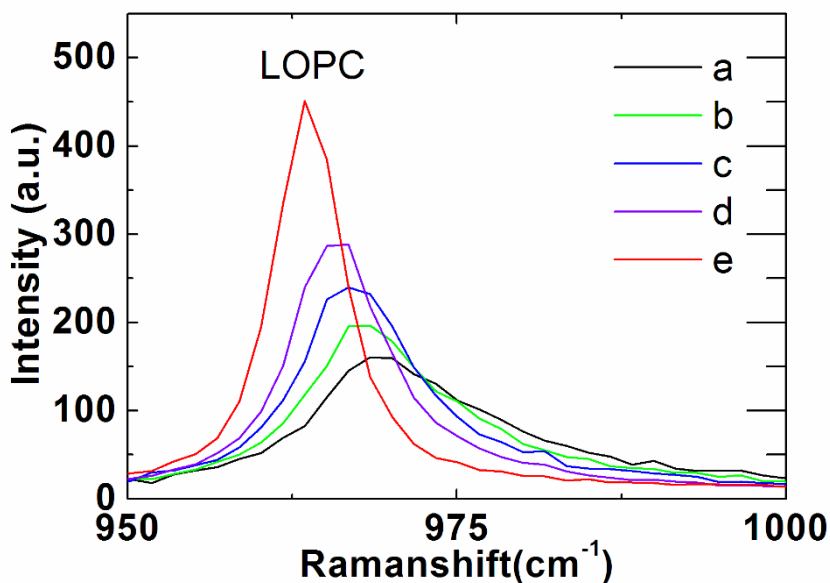


Figure 2. LOPC modes of points a, b, c, d and e.

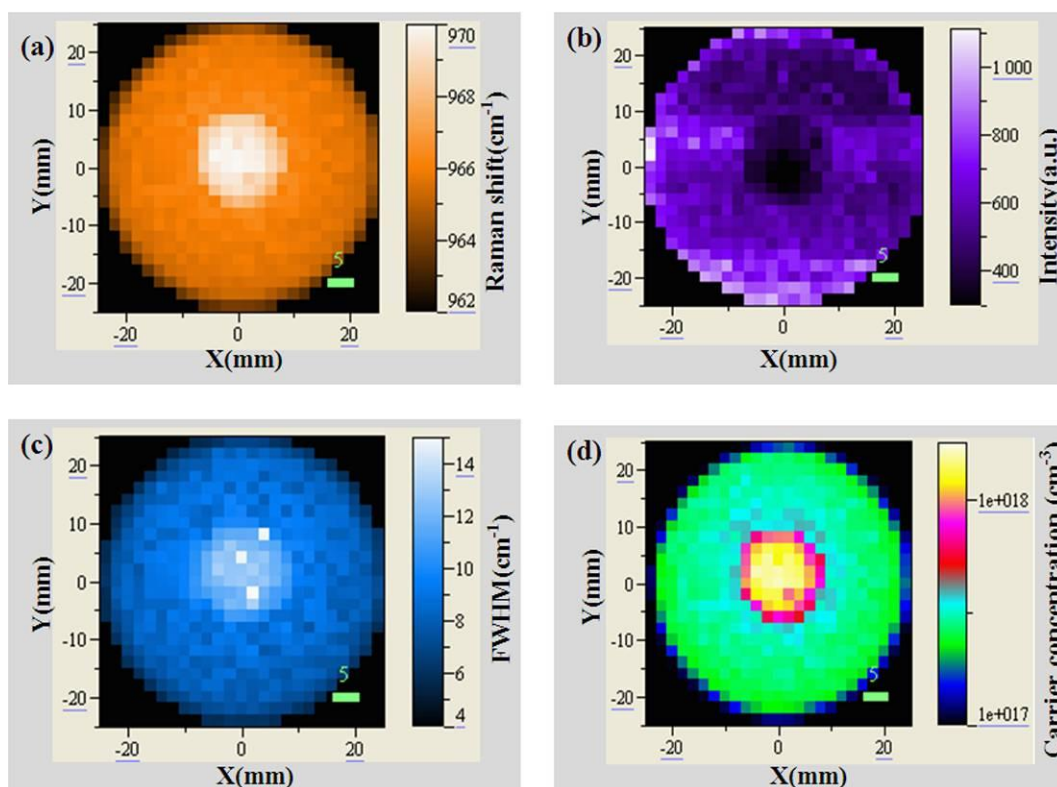


Figure 3. Raman mappings of LOPC modes. (a) peak position; (b) intensity; (c) FWHM; (d) simulated carrier concentration distribution.

Nakashima *et al.*[19,25] plotted the peak frequency of the LOPC mode as a function of the carrier concentration on a logarithmic scale, and they found there is a very simple relationship between the carrier concentration and the LOPC mode frequency relative to the bare LO phonon frequency in pure 4H-SiC in units of cm^{-1} . It can be expressed by

$$n = 1.25 \times 10^{17} (\text{cm}^{-3}) (\omega_{LOPC} - \omega_L)^{1.0} = 1.25 \times 10^{17} (\Delta\omega)^{1.0} \quad (2)$$

Therefore, the carrier concentration distribution can be simulated according to the Raman mapping results of LOPC mode, as shown in Fig. 3d. The carrier concentration decreases monotonously from center to edge of the wafer. This result agrees well with the resistivity measurement. As the B concentration was almost the same through the whole wafer in SiC growth, the image of carrier concentration distribution was a response of the N impurity in the wafer.

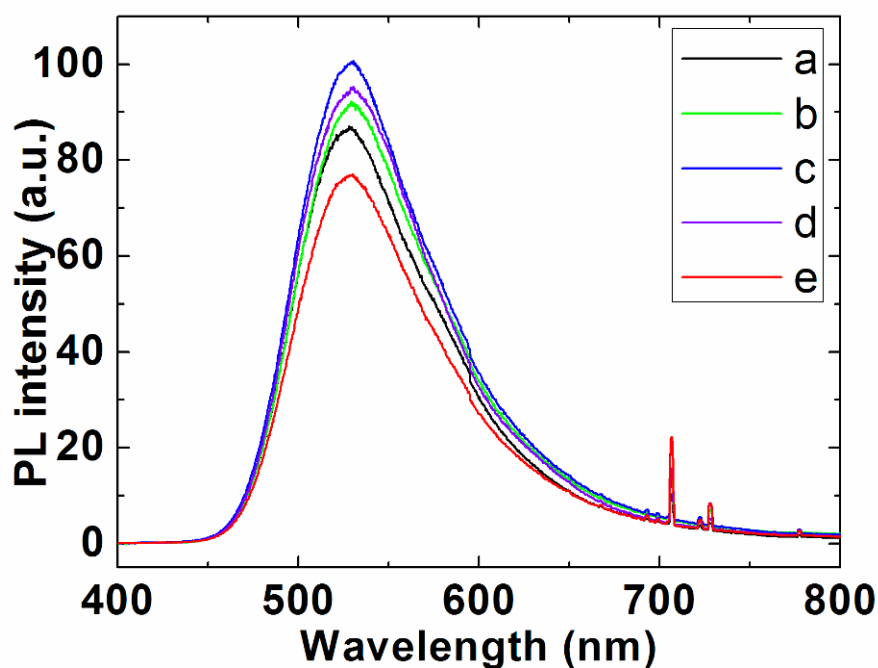


Figure 4. PL spectra of points a, b, c, d and e.

Photoluminescence (PL) was excited by a 325 nm laser with a power of 0.28 mW. Both single point and mapping scan were performed at room temperature. The PL results of points a, b, c, d and e were shown in Fig.4. The results showed that PL spectrum has a peak wavelength of about 538 nm (2.3 eV) and FWHM of about 104 nm. It covers the most of visible light region. This result indicates that N-B doped 4H-SiC prepared by PVT method was a feasible fluorescent substrate.

The PL mapping results were shown in Fig.5. The results showed that the emission has the peak position of 538 ± 3 nm and FWHM of 104 ± 1 nm across the substrate. Despite of the intensity differences, the peak positions of the spectra and the FWHM are kept almost the same through the whole wafer. From the above results, one can see that the carrier concentration difference only affect the emission intensity but do not cause the variation of the peak wavelength and FWHM. Therefore, the shape of PL spectrum usually depends on the Coulomb interaction and phonon coupling rather than the carrier concentration[26,27].

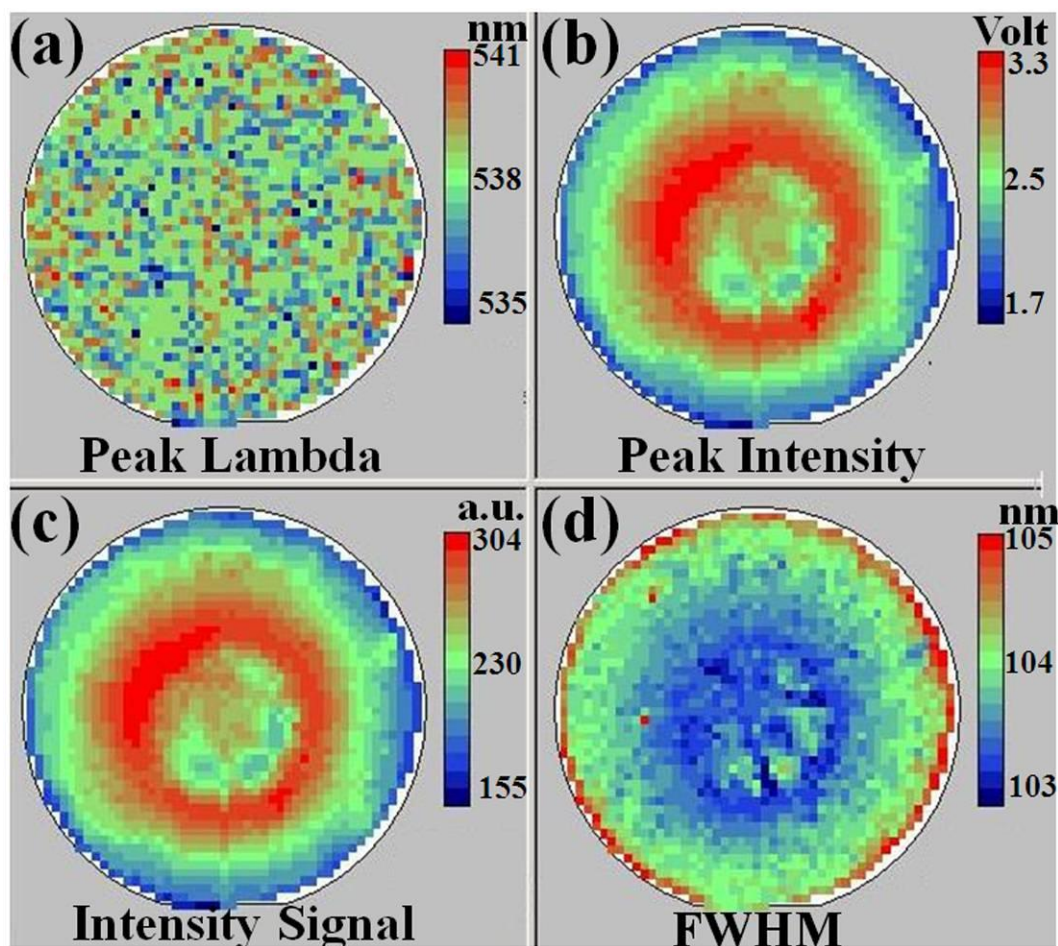


Figure 5. PL mappings. (a) peak wavelength; (b) peak intensity; (c) intensity signal; (d) FWHM.

The dependence of the DAP emission intensity on doping concentration could be explained by using band diagram with Fermi-Dirac statistics[17,28,29].

The DAP recombination rate R_{DA} can be described by the following equation

$$R_{DA} \propto N_D \times F_D \times N_A \tag{3}$$

where F_D is the occupancy probability of an electron on donor states, nearly constant for n-type SiC. From above equation, we can see that high donor and acceptor doping concentrations will result in intense DAP recombination. Higher DAP recombination rate R_{DA} will be achieved while the concentration of N increases, which will result in intense luminescence. Therefore, the most intense PL emission should appear at the center of the wafer. But in our experiment, the most intense emission located at the region between edge and center, about $r/2$ away from center of the wafer. The intensity of PL increases from the edge to $r/2$ of the wafer, and decreases from $r/2$ to center.

The carrier concentration has major influence on the absorption coefficient α . The Drude model for carrier absorption predicts a linear relationship between the absorption coefficient and the charge carrier concentration. Weingartner *et al.* plotted such a relationship [30-34]

$$\alpha = \alpha_0 + k \times n = (2.4 \pm 1.3)cm^{-1} + (3.6 \pm 0.1) \times 10^{-17} cm^{-2} \times n \tag{4}$$

Where n is the free carrier concentration. The absorption coefficient increases with carrier concentration. With the increases of N concentration, the DAP emission will be enhanced. But at the same time, a higher absorption rate by free carrier will be achieved. Therefore, the PL intensity will be reduced while the increase of absorption rate is larger than that of the DAP emission as shown in the PL result of our experiment. So in order to get the satisfying fluorescent 4H-SiC substrates, which has the most intense and uniform PL emission, growth process needed to be improved to optimize the doping of N and B.

4. CONCLUSIONS

Nitrogen-Boron doped 4H-SiC single crystal was prepared by physical vapor transport method. It was found that the resistivity of the wafer increases gradually from center to edge, which agree with the carrier concentration distribution simulated by Raman spectra. The PL mapping for DA 4H-SiC shows a peak wavelength of about 538 nm with FWHM about 104 nm. The intensity of PL spectra does not increase linearly with the nitrogen doping concentration because with the increase of the DAP recombination, the absorption caused by carrier enhanced at the same time.

ACKNOWLEDGEMENTS

This work was supported by National Basic Research Program of China under grant No. 2011CB301904 and No. 2009CB930503, Natural Science Foundation of China under grant No. 51021062 and 11134006, Independent Innovation Foundation of Shandong University under grant No. 2011GN057.

References

1. H. Yamamoto, *Proc. SPIE*. 7598 (2010) 759808.
2. H. Kuo, C. Hung, H. Chen, K. Chen, C. Wang, C. Sher, C. Yeh, C. Lin, C. Chen and Y. Cheng, *Opt. Express*. 19 (2011) A930.
3. H. Menkara, R. A. Gilstrap Jr., T. Morris, M. Minkara, B. K. Wagner and C. J. Summers, *Opt. Express*. 19 (2011) A972.
4. H. Zhao, J. Zhang, G. Liu and N. Tansu, *Appl. Phys. Lett.* 98 (2011) 151115.
5. T. J. Prosa, P. H. Clifton, H. Zhong, A. Tyagi, R. Shivaraman, S. P. DenBaars, S. Nakamura and J. S. Speck, *Appl. Phys. Lett.* 98 (2011)191903.
6. C. Wetzel and T. Detchprohm, *Opt. Express*. 19 (2011) A962.
7. H. Zhao, G. Liu, J. Zhang, J. D. Poplawsky, V. Dierolf and N. Tansu, *Opt. Express*. 19 (2011) A991.
8. X. Li, R. Song, Y. Ee, P. Kumnorkaew, J. F. Gilchrist and N. Tansu, *IEEE Photon. J.* 3 (2011) 489.
9. J. Zhang, H. Zhao and N. Tansu, *Appl. Phys. Lett.* 97 (2010) 111105.
10. J. Zhang, H. Zhao and N. Tansu, *Appl. Phys. Lett.* 98 (2011)171111.
11. T. Kolbe, A. Knauer, C. Chua, Z. Yang, S. Einfeldt, P. Vogt, N. M. Johnson, M. Weyers and M. Kneissl, *Appl. Phys. Lett.* 97 (2010)171105.
12. K. Hazu and S. F. Chichibu, *Opt. Express*. 19 (2011) A1008.

13. J. H. Strait, P. A. George, J. Dawlaty, S. Shivaraman, M. Chandrashekhar, F. Rana and M. G. Spencer, *Appl. Phys. Lett.* 95 (2009) 051912.
14. G. Xuan, P. C. Lv, X. Zhang, J. Kolodzey, G. Desalvo and A. Powell, *J. Electron. Mater.* 37 (2008) 726.
15. M. Mirzaei and M. Mirzaei, *J. Mol. Model.* 17 (2011) 527.
16. S. Choudhary and S. Qureshi, *Phys. Lett. A* 375 (2011) 3382.
17. S. Kamiyama, T. Maeda, Y. Nakamura, M. Iwaya, H. Amano and I. Akasaki, *J. Appl. Phys.* 99 (2006) 093108.
18. Mikael Syväjärvi, *Adv. Mat. Lett.* 3(3) (2012) 175.
19. S. Nakashima, T. Kitamura, T. Kato, K. Kojima, R. Kosugi, H. Okumura, H. Tsuchida and M. Ito, *Appl. Phys. Lett.* 93 (2008) 121913.
20. G. Irmer, V. V. Toporov, B. H. Bairamov, and J. Monecke, *Phys. Status Solidi. B* 119 (1983) 595.
21. H. Yugami, S. Nakashima, A. Mitsuishi, A. Uemoto, M. Shigeta, K. Furukawa, A. Suzuki and S. Nakajima, *J. Appl. Phys.* 61 (1987) 354.
22. Hiroshi Harima, Hirokazu Sakashita, Toshiaki Inoue and Shin-ichi Nakashima, *J. Cryst. Growth.* 189 (1998) 672.
23. Joshua D. Caldwell, Orest J. Glembocki, Sharka M. Prokes, Evan R. Glaser and Karl D. Hobart, *J. Appl. Phys.* 101 (2007) 093506.
24. Hiroshi Harima, Shin-ichi Nakashima and Tomoki Uemura, *J. Appl. Phys.* 78 (2007) 1996.
25. S. Nakashima, T. Kitamura, T. Mitani, and H. Okumura, *Phys. Rev. B.* 76 (2007) 245208.
26. M. Ohishi, *Jpn. J. Appl. Phys.* 25 (1986) 1546.
27. P. B. Aume, F. Kubacki, and J. Gutowski, *J. Cryst. Growth.* 138 (1994) 266.
28. Satoshi Kamiyama, Motoaki Iwaya, Tetsuya Takeuchi, Isamu Akasaki, Mikael Syväjärvi, and Rositza Yakimova, *J. Semicond.* 32 (2011) 013004.
29. Yiyu Ou, Valdas Jokubavicius, Satoshi Kamiyama, Chuan Liu, Rolf W. Berg, Margareta Linnarsson, Rositza Yakimova, Mikael Syväjärvi and Haiyan Ou, *Opt. Mater Express.* 1 (2011) 1439.
30. R. Weingartner, P. J. Wellmann, M. Bickermann, D. Hofmann, T. L. Straubinger, and A. Winnacker, *Appl. Phys. Lett.* 80 (2002) 70.
31. Z.G. Herro, B.M. Epelbaum, R. Weingartner, M. Bickermann, P. Masri, and A. Winnacker, *J. Cryst. Growth.* 270 (2004) 113.
32. P.J. Wellmann and R. Weingartner, *Materials Science and Engineering.* B102 (2003) 262,.
33. P.J. Wellmann, R. Weingartner, M. Bickermann, T.L. Straubinger and A. Winnacker, *Materials Science and Engineering.* B91–92 (2002) 75 .
34. R. Weingartner, M. Bickermann, S. Bushevoy, D. Hofmann, M. Rasp, T.L. Straubinger, P.J. Wellmann and A. Winnacker, *Materials Science and Engineering.* B 80 (2001) 357 .